



Cyclic response of infilled RC frames with window and door openings: Experimental results and damage interpretation

Fabio Di Trapani¹  | Nisar Ali Khan² | Lin Zhou³  | Cristoforo Demartino² | Giorgio Monti³

¹Politecnico di Torino, Dipartimento di Ingegneria Strutturale Edile e Geotecnica, Turin, Italy

²Roma Tre University, Department of Architecture, Rome, Italy

³Sapienza Università di Roma, Dipartimento di Ingegneria Strutturale e Geotecnica, Rome, Italy

Correspondence

Fabio Di Trapani, Dipartimento di Ingegneria Strutturale, Edile e Geotecnica, Politecnico di Torino, Corso Duca degli Abruzzi 24, 10129, Turin, Italy.
Email: fabio.ditrapani@polito.it

Lin Zhou, Dipartimento di Ingegneria Strutturale e Geotecnica, Sapienza Università di Roma, Rome, Italy.
Email: linzhou1990@yeah.net

Abstract

The paper presents the results of an experimental investigation assessing the influence of the openings typology and position on the cyclic response of masonry-infilled reinforced concrete frames. The experimental program consisted of seven 2/3 scale square frame specimens infilled with hollow clay bricks, which were subjected to quasi-static lateral cyclic tests up to large drifts. A reference bare frame was also tested for comparison. The specimens included solid infill walls, infills with door openings, and infills with window central and eccentric openings. The experimental responses of the specimens were analyzed in terms of strength, stiffness, energy dissipation capacity, and equivalent damping, and were compared to those of the reference bare frame and fully infilled frame. Results revealed a significant modification of the resisting mechanisms as a function of the typology and position of the openings with respect to the case of a fully infilled frame, although the lateral resisting capacity was not substantially modified. On the other hand, it was observed that the achievement of the limit state thresholds occurred at substantially different interstorey drifts, indicating different damage metrics. Simple regression analyses, based on the experimental results of this study and from the literature, were finally conducted to interpret the modification of the peak force and of the corresponding drift as a function of synthetic parameters defining the opening arrangement.

KEYWORDS

energy dissipation, experimental testing, hysteretic response, infilled frames, masonry, openings, reinforced concrete

1 | INTRODUCTION

The decisive influence of masonry infills on the seismic performance of frame structures has been extensively studied through post-earthquake damage observations, experimental testing, and numerical simulations. These studies have conclusively demonstrated that masonry infills significantly impact overall seismic performance parameters, including strength, stiffness, ductility, and collapse modes. Therefore, the inclusion of masonry infills in seismic safety assessments of existing structures and the design of new ones is imperative. In recognition of this, a significant number of researchers have conducted extensive experimental investigations in this field over the past 50 years. In a recent paper, Huang et al.,¹ estimate 264 tests carried out on reinforced concrete and steel infilled frames loaded in-plane. Numerous valuable

NOVELTY

- Infilled frames with central/eccentric window and door openings were cyclically tested up to large drifts to assess their strength, stiffness, and energy dissipation with respect to bare and fully infilled frames.
- The dependence of the mechanical response on the typology and position of the openings was focused as well as the development of alternative resisting mechanisms.
- Damage metrics indicating the reference limit state thresholds were reconsidered as a function of the opening arrangement.
- Empirical expressions were defined to interpret the modification of the peak response depending on the opening typology.

experimental campaigns have been conducted in the field of reinforced concrete frames with solid infills, including those by Mehrabi and Shing,² Calvi and Bolognini,³ Al-Chaar,⁴ Papia et al.,⁵ Colangelo,⁶ Da Porto et al.,⁷ Cavaleri and Di Trapani,⁸ Bergami and Nuti,⁹ Verderame et al.,¹⁰ and Morandi et al.¹¹ These studies have contributed significantly to the understanding of the behavior of reinforced concrete frames with solid infills under seismic loading. At the same time, several attempts to reproduce the experimental responses by analytical and numerical approaches have been performed using refined finite element micro-models (e.g., Mehrabi & Shing,¹² Koutromanos et al.,¹³ Calì & Pantò,¹⁴ Di Trapani et al.,¹⁵ Milanese et al.,¹⁶ Di Trapani et al.¹⁷), simplified equivalent strut macro-models (e.g., Bertoldi et al.,¹⁸ Panagiotakos & Fardis,¹⁹ Dolsek & Fajfar,²⁰ Rodrigues et al.,²¹ Di Trapani et al.,¹⁵ De Risi et al.,²² Liberatore et al.,²³ Di Trapani²⁴), or multi-strut macro-models Chrysostomou et al.,²⁵ El-Dakhakhni et al.,²⁶ Crisafulli and Carr,²⁷ Fiore et al.,²⁸ Jeon et al.,²⁹ and Di Trapani et al.³⁰ Comprehensive dataset collections have been also provided by Huang et al.,¹ Blasi et al.,³¹ and De Risi et al.²²

In recent decades, parallel studies have been undertaken to evaluate the impact of openings on the seismic response of infilled frames. These studies have employed both experimental testing and numerical simulations to investigate the behavior of steel and reinforced concrete infilled frames. The results of these investigations have demonstrated that, in the case of door or window openings, infills are still capable of providing additional strength and stiffness, though this is dependent on the opening percentage and location within the frame. Additionally, it is found that the size and location of openings have a significant effect on the seismic performance of infilled frames. Available tests on infilled frames with openings are significantly less than those made for solid ones (Mohammadi & Nikfar³²), among these Dawe and Seah,³³ Mosalam et al.,³⁴ Tasnimi and Mohebkah³⁵ tested one-storey steel-infilled frames, while most of the experimental works focused on reinforced concrete infilled frames (e.g., Kakaletsis & Karayannis,^{36–38} Blackard et al.,³⁹ Sigmund & Penava,⁴⁰ Zhai et al.,⁴¹ Mansouri et al.,⁴² Morandi et al.,⁴³ Basha et al.⁴⁴). Full-scale reinforced concrete multi-storey frames including both solid infills and infills with openings were also tested by Carvalho and Coelho,⁴⁵ Al-Chaar et al.,⁴⁶ and Stavridis et al.⁴⁷ In consideration of the results from the experimental tests, different authors provided empirical relationships to effectively modify the equivalent strut approach to consider the strength and stiffness reduction due to the presence of the openings. These analytical expressions generally related a reduction coefficient ($r \leq 1$) to a parameter that accounts for the opening ratio with respect to the area of the entire infill wall. In most cases the ratio A_o/A_i was used, where A_o is the area of the opening and A_i is the area of the infill. This reduction coefficient is applied to the width (w) of the equivalent strut evaluated for a solid infilled frame. Among these approaches, it is worth mentioning those by Dawe and Seah,³³ Durrani and Luo,⁴⁸ Papia et al.,⁵ Al-Chaar et al.,⁴⁶ Asteris,⁴⁹ Mondal and Jain,⁵⁰ Tasnimi and Mohebkah,³⁵ Decanini et al.,⁵¹ and Asteris et al.,⁵² while similar prescriptions are given by some technical standards such as ASCE/SEI 41-13⁵³ and NZSEE.⁵⁴ It has been well established through experimental and numerical studies that the type and position of openings within infilled frames have a significant impact on the seismic response in terms of strength, stiffness, and collapse mechanisms. However, the majority of existing empirical relationships used to model this behavior only take into account the opening area as an input parameter, neglecting the influence of opening position and type on the seismic response of infilled frames. This simplified assumption is a result of the limited understanding of the underlying damage mechanisms. As such, further research is needed to develop more comprehensive models that take into account these factors. To achieve this, a more detailed understanding of the damage mechanisms associated with infilled frames is necessary. This knowledge can then be used to establish new analytical formulations that can be employed in the next generation of standard building codes.

TABLE 1 Typological and geometrical features of the specimens.

Specimen	Scale	Type of opening	Position of the opening	Type of masonry	l_i (mm)	h_i (mm)	l_o (mm)	h_o (mm)	l_l (mm)	l_r (mm)	h_t (mm)	h_b
BF	2:3	–	–	Bare frame	–	–	–	–	–	–	–	–
FIF	2:3	No opening	No opening	Hollow clay bricks	2200	2100	0	0	0	0	0	0
CW-F1	2:3	Window	Central	Hollow clay bricks	2200	2100	900	800	650	650	650	650
CW-F2	2:3	Window	Central	Hollow clay bricks	2200	2100	900	800	650	650	650	650
SW-F1	2:3	Window	Eccentric	Hollow clay bricks	2200	2100	900	800	200	1100	650	650
SW-F2	2:3	Window	Eccentric	Hollow clay bricks	2200	2100	900	800	200	1100	650	650
CD-F1	2:3	Door	Central	Hollow clay bricks	2200	2100	750	1650	725	725	450	0
CD-F2	2:3	Door	Central	Hollow clay bricks	2200	2100	750	1650	725	725	450	0

Focusing on reinforced concrete infilled frames with openings, this study provides an experimental investigation on the influence of the opening typology and position on the lateral response of infilled frames. Seven 2/3 scaled square infilled frame specimens arranged with hollow clay bricks have been subjected to quasi-static cyclic tests up to large drifts. The specimens included solid infill walls, infills with door openings, and infills with window central and eccentric openings. To provide a comprehensive understanding of the impact of openings on the seismic response of infilled frames, an additional bare frame specimen was also tested as a reference. The hysteretic responses of the infilled frames with openings were then compared to that of the bare frame and of the specimens with solid infills in terms of strength, stiffness, energy dissipation capacity, failure mechanisms, and damage thresholds. The results were used to provide a deeper understanding of the modification of the mechanical response of infilled frames with window and door openings, focusing particularly on the overall response parameters and the damage mechanisms activated as a function of the typology of the openings and their position within the infill. It was also highlighted that the damage metrics commonly adopted to assess the limit states of solid infills need to be reconsidered in the case of window and door openings. The experimental results were collected and analyzed along with available literature data to provide an empirical estimation of the expected peak response modification (peak resistance and peak interstorey drift) of infilled frames with openings in comparison to fully infilled frames.

2 | EXPERIMENTAL PROGRAM

2.1 | Specimen details

The experimental program entailed subjecting eight 2/3 scaled specimens to a quasi-static cyclic loading protocol. The specimens were designed according to the Chinese standard GB 50011-2010⁵⁵ and are representative of a sub-frame extracted from a common three-storey residential building located in a moderate-to-low seismic hazard region. The eight specimens included a bare frame, a frame with a solid infill and six infilled frames with openings. The detailed experimental program is reported in Table 1. The geometric dimension of the specimens appearing in Table 1 refer to the scheme depicted in Figure 1. The infills had a total dimension of 2200 × 2100 mm and were arranged with two wythes of hollow clay masonry bricks (230 × 110 × 80 mm). The two wythes of masonry are made of brick layers arranged in parallel, alternatively along the layer length and along its thickness, in order to realize an effective transverse connection (Figure 2). The adopted brick typology, as well as the arrangement of the masonry, is quite common in China and in the neighboring countries of South Asia, such as Pakistan, India, and Iran. The mortar layers had a thickness of about 10 mm. The bricks were unscaled with respect to the overall specimen's scale (2/3), but they were small enough to consider the scale effects to be negligible. The reinforced concrete frame used in all tests had the geometrical and reinforcement details depicted in Figure 2. The specimens were built by casting the concrete frames first. The construction of the infills started after a 28-day curing period of the concrete. The arrangement of the infills provided filling the interface mortar joints between the masonry and the concrete frame to ensure contact during the tests. In this construction phase, special care was addressed to filling the interface joint between masonry and top beam.

Infilled frames with openings consisted of 3 typologies, central window openings (CW), side window openings (SW), and central door openings (CD). Two replicas of each typology (F1 and F2) were arranged. Geometrical schemes of the infilled frame specimens are provided in Figure 3. The opening ratio (A_o/A_i) was 15.6% for the window openings and 26.8%

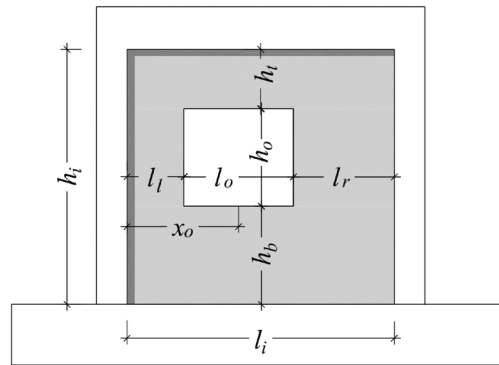


FIGURE 1 Reference geometrical parameters of an infilled frame with an opening in a generic position.

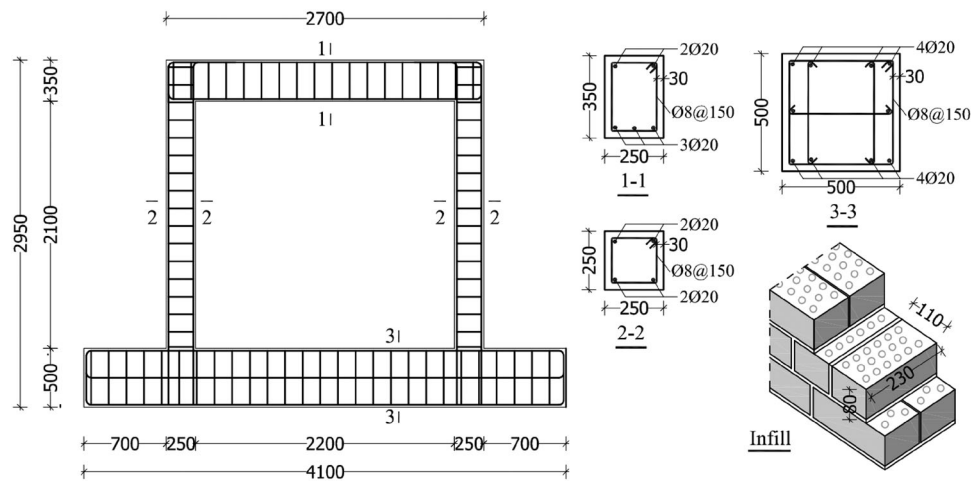


FIGURE 2 Reinforcement details of the frame and arrangement of the masonry (dimensions in mm).

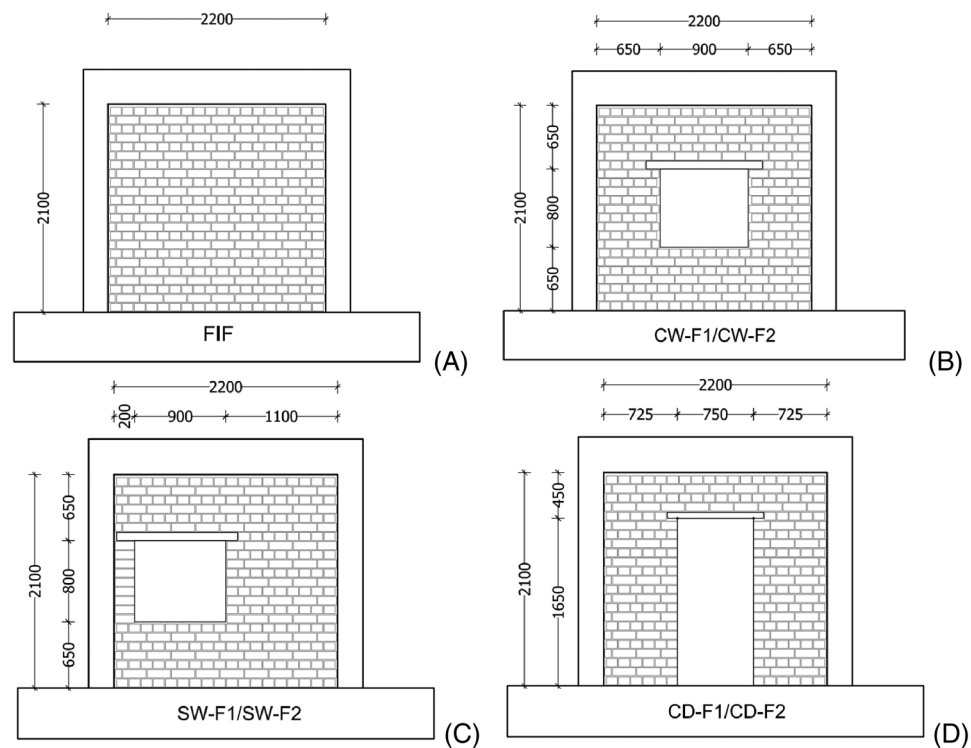


FIGURE 3 Geometric details of specimens: (A) IF; (B) CW; (C) SW; (D) CD. Dimensions in mm.

TABLE 2 Geometrical ratios of the infilled frame specimens with the openings.

Specimen	A_o/A_i (%)	l_o/l_i (–)	h_o/h_i (–)	x_o/l_i (–)	h_i/h_i (–)
CW-F1/CW-F2	15.6%	0.41	0.38	0.50	0.31
SW-F1/SW-F2	15.6%	0.41	0.38	0.30	0.31
CD-F1/CD-F2	26.8%	0.34	0.79	0.50	0.21

**FIGURE 4** Brick units: (A) view from the top; (B) side view; (C) compressive test.**TABLE 3** Mechanical properties of materials.

Specimen	Concrete	ϕ 20 Steel		ϕ 8 Steel		Brick	Mortar
	f_c (MPa)	f_y (MPa)	f_t (MPa)	f_y (MPa)	f_t (MPa)	f_b (MPa)	f_{mr} (MPa)
#1	13.78	441	638	488	620	10.5	5
#2	13.95	438	618	569	699	11.6	2.6
#3	13.33	431	668	423	646	12	3.4
#4	13.87	420	202	460	654	8.7	3.4
#5	13.65	491	616	432	570	13.2	4.4
#6	12.62	428	585	468	643	12.2	1.6
#7						26.9	3.8
#8						14.4	3.6
#9						14.6	2.3
#10						20.2	2.2
#11							2.5
#12							4.2
Mean	13.53	441.50	554.50	473.33	638.67	14.43	3.25
Std. Dev.	0.50	25.37	174.85	52.56	42.45	5.35	1.02
COV	4%	6%	32%	11%	7%	37%	31%

for the door openings. The eccentricity of the openings was defined as the ratio between the horizontal distance of the center of the openings (x_o) and the length of the infill (l_i) (eccentricity ratio). This ratio results in 0.5 for central openings. The openings of specimen SW were characterized by an eccentricity ratio of 0.3. Additional geometrical ratios identifying the opening position within the infills are summarized in Table 2.

2.1.1 | Material properties

Comprehensive material tests were carried out. Material tests included compressive tests on concrete $150 \times 150 \times 150$ mm cubes, mortar $50 \times 50 \times 50$ mm cubes, tensile tests on steel rebars, compressive tests on bricks. Bricks had a 20% opening percentage (Figure 4A,B). Compressive tests on bricks were carried out parallel to the direction of the holes (Figure 4C) according to the ASTM C67⁵⁶ standard. The results of the tests are reported in Tables 3 and 4. The average compressive strength of the bricks (f_b) resulted in 14.43 MPa.

TABLE 4 Mechanical properties of the infill masonry.

Specimen	Compressive tests parallel to the holes f_m (MPa)	Diagonal shear tests f_v (MPa)
#1	3.00	0.352
#2	3.55	0.321
#3	3.52	0.395
Average	3.36	0.356
Standard deviation	0.31	0.04
Coeff. of variation	9%	10%
	Average elastic modulus parallel to the holes E_m (MPa)	Average shear modulus G_m (MPa)
	3730	318.8

2.2 | Masonry properties

Three masonry prisms having dimensions of $900 \times 750 \times 230$ mm were tested in compression according to the ASTM E447-97⁵⁷ standard. The tests were carried out along the direction of the holes of the bricks, which is orthogonal to the mortar bed joints (Figure 5A). The average compressive strength of the masonry specimens (f_m) was determined to be 3.36 MPa. The average elastic Young's modulus (E_m) was 3730 MPa. A view of a masonry wall specimen at the end of the tests is provided in Figure 5B. Compressive tests of masonry prisms orthogonally to the direction of the hole were also carried out. However, the outcomes of these tests are omitted in this paper due to discrepancies stemming from anomalies within the specimens. Despite these data inconsistencies, the horizontal resistance of the masonry (f_{mh}) can be estimated according to the Eurocode 6 formula as 75% of the vertical one. In addition, diagonal shear tests were carried out on masonry wall specimens having dimensions $620 \times 620 \times 230$ mm (Figure 6A). The tests allowed evaluating the average shear resistance in absence of compressive loads by dividing the peak load by the diagonal transverse area of the specimen, that is the diagonal length by the thickness of specimens. The shear resistance resulted in $f_{vm} = 0.356$ MPa, while the average shear modulus was $G_m = 318.8$ MPa. The normal stress versus normal strain ($\sigma-\epsilon$) and tangential stress versus angular deformation diagrams ($\tau-\gamma$) were also obtained and are depicted in in Figure 7. For both compressive and shear tests, limited variability of the peak strength was observed. In terms of strains, similar results were obtained by the specimens tested in compression, while significant variability in terms of angular deformation was recognized for specimens subject to shear test. This trend was justified by the abrupt formation of large cracks crossing the measurement system reference points. However, this did not affect the evaluation of the peak shear strength, which was affected by a low coefficient of variation (10%), that is in the same order of magnitude of that of the compressive tests (9%).

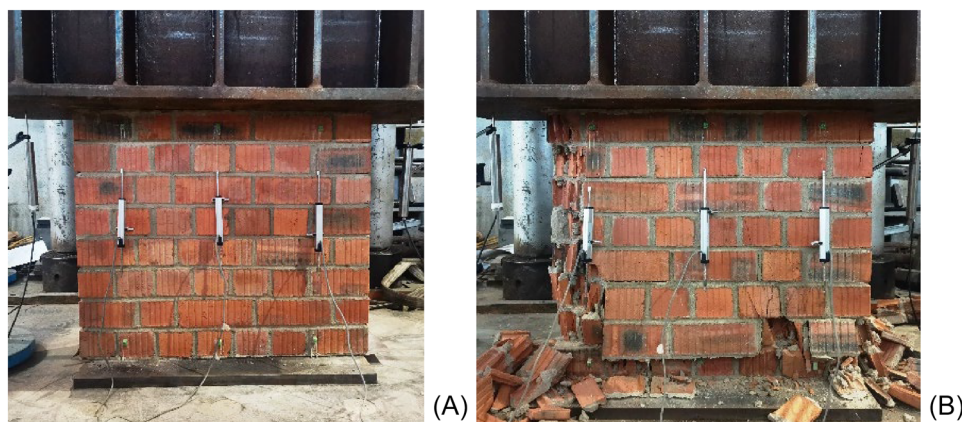


FIGURE 5 Compressive tests on masonry prisms: (A) specimen at the beginning of the test; (B) specimen at the end of the test.

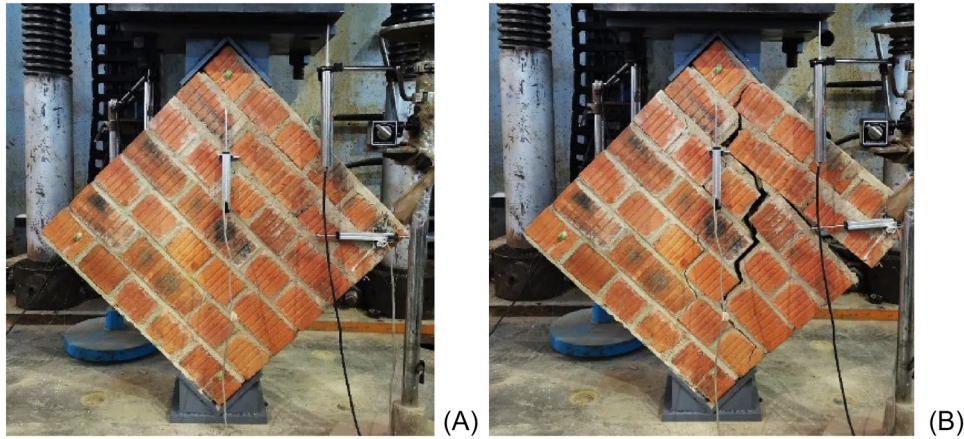


FIGURE 6 Diagonal shear tests on masonry: (A) specimen at the beginning of the test; (B) specimen at the end of the test.

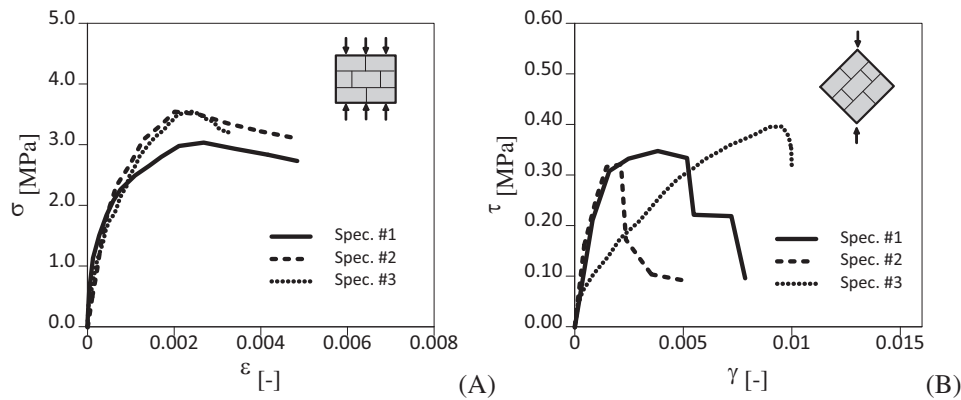


FIGURE 7 Stress-strain responses from tests on masonry prisms: (A) compressive tests; (B) diagonal shear tests.

2.3 | Test setup and instrumentation

All specimens were tested in the structural lab of the Zhejiang Technical University (Hangzhou, China). A scheme of the test setup is shown in Figure 8A, while a picture of a specimen in the testing apparatus is provided in Figure 8B. The horizontal lateral load was applied at mid-height of the beam by a double-action hydraulic actuator, connected on one side to the reaction wall and on the other one to the steel beam with a hinged connection. The hydraulic jack had a stroke of ± 250 mm and a nominal load capacity of ± 2000 kN. To transfer the horizontal force to the frame during reverse loading cycles, a system of two steel plates and four prestressed rebars was applied to the steel beam. Additionally, a concentrated vertical load was applied to the RC columns via two independent hydraulic jacks. The vertical load, which was constant and equal to 390 kN, was applied using two vertical hydraulic jacks. The vertical load was transferred from the jacks to the specimen via a horizontal steel beam, which was in contact with the columns of the frame via two steel plates. These plates enabled the distribution of the vertical load to the columns (195 kN per column, corresponding to an axial load ratio of 0.2) in a manner that replicated the effects of gravity loads.

To constrain vertical displacements and rotation, the foundation of the specimen was fixed to the strong floor with two steel beams through 50 mm diameter high-strength threaded rods. To further prevent any lateral movement, the base beam was braced against the reaction wall using an anti-slip device. Each specimen was subject to an imposed cyclic displacement protocol of 30 cycles. Each cycle was repeated 3 times for each target displacement. The displacement testing protocol is illustrated in Figure 9. The target displacements started by ± 10 mm and were increased by 10 mm after completing each group of three cycles. The maximum displacement achieved was 100 mm. The corresponding interstorey drift ranges from 0.47% to 4.7%. For all the tests, the lateral force versus top displacement response was recorded. The displacement testing protocol is also illustrated in Figure 9.

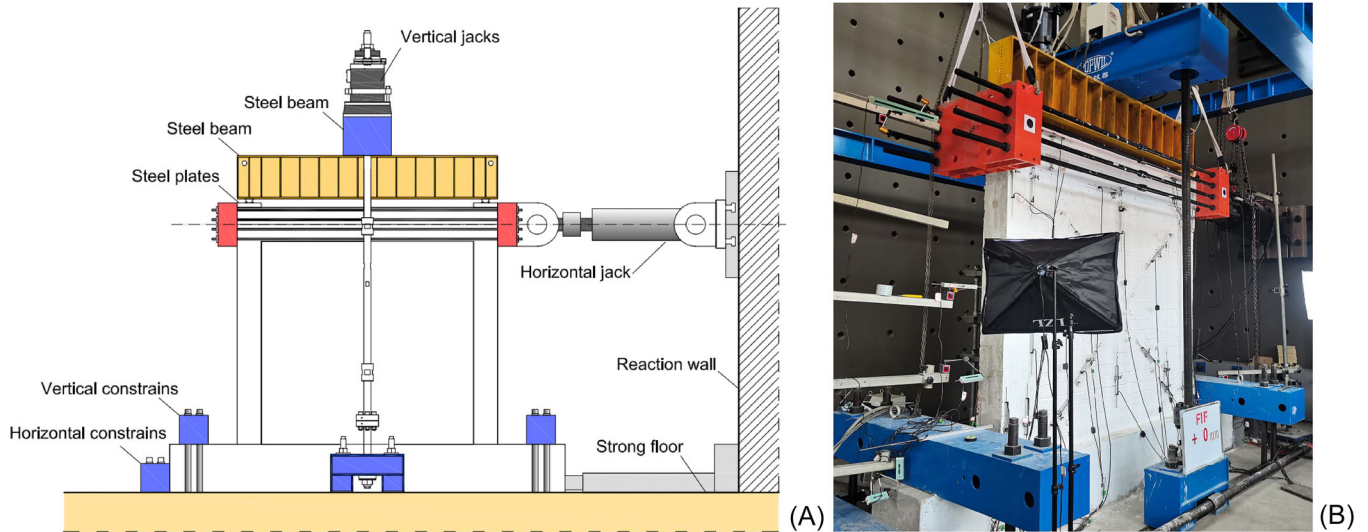


FIGURE 8 Test setup and instrumentation: (A) scheme of the test setup; (B) view of a specimen in the testing apparatus.

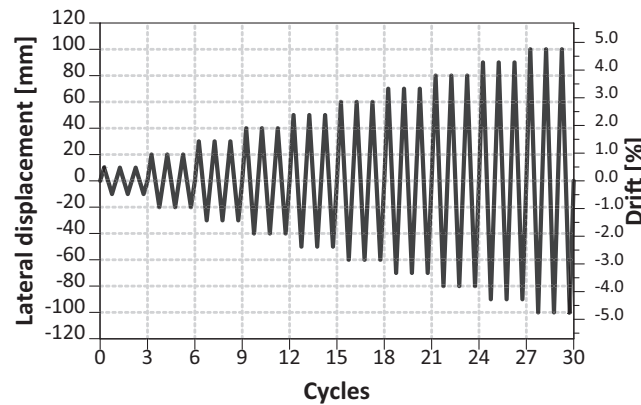


FIGURE 9 Cyclic displacement testing protocol.

3 | EXPERIMENTAL RESULTS

The results were analyzed and compared in terms of strength, stiffness, energy dissipation capacity, and damage evolution. The study specifically investigated the influence of opening typology and position on the response, with a specific focus on the modification of response in comparison to the bare frame and the fully infilled frame cases. The cyclic responses of the specimens are depicted in Figure 10. A comprehensive analysis of the results revealed that all the infilled frame specimens exhibited a significant modification of response in comparison to bare frame specimens, indicating a decisive role of the infills. For both cases of infilled frames with and without openings, an overall increase in stiffness and resistance was observed. The peak and post-peak responses of the infilled frames were dependent on the specific test, indicating a variable evolution during testing as function of the arrangement. Further interpretation of the test outcomes is provided in subsequent sections.

3.1 | Strength, stiffness, and displacement capacity

Figure 11A provides the backbone curves (positive and negative) for the different specimens where strength and stiffness are more clearly observable. Strength and stiffness were evaluated on the average (positive and negative) backbone curves (Figure 11B). The initial stiffness (K_0) of the specimens was evaluated as the slope of the line joining the origin to the point at the initial cracking stage, denoted by the first change of the slope. Table 5 summarizes the initial stiffness values, the

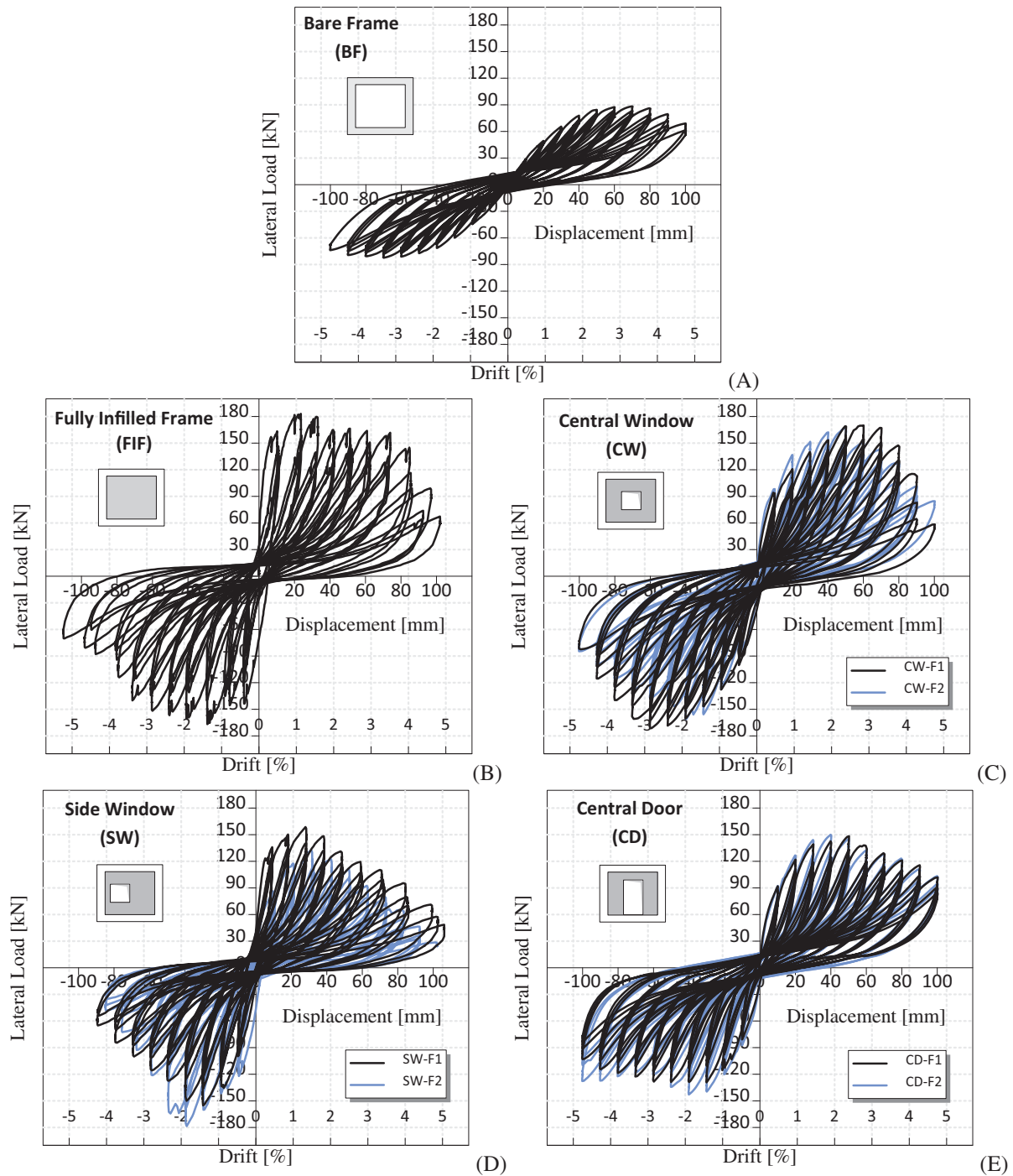


FIGURE 10 Cyclic responses of the specimens: (A) bare frame (BF); (B) fully infilled frame (FIF); (C) central window (CW); (D) side window (SW); (E) central door (CD).

ratios between the initial stiffness of the infilled frames and that of the bare frame (K_0/K_{B0}), and the ratios between the initial stiffness of the infilled frames with the openings and that of the fully infilled frame ($K_0/K_{FI,0}$). As it can be observed, the initial stiffness of the fully infilled frame was significantly higher (about 21 times) than that of the bare frame. The presence of the openings produced an initial stiffness reduction of about 70% with respect to the stiffness of the fully infilled frame. The stiffness of the infilled frames with openings was still higher by about 6 times than the BF stiffness. It is noteworthy that, despite the different opening typologies and positions, the infilled frame specimens with the openings showed similar initial stiffness. This was on average 27% of the initial stiffness of the fully infilled frame (Table 5 and Figure 12).

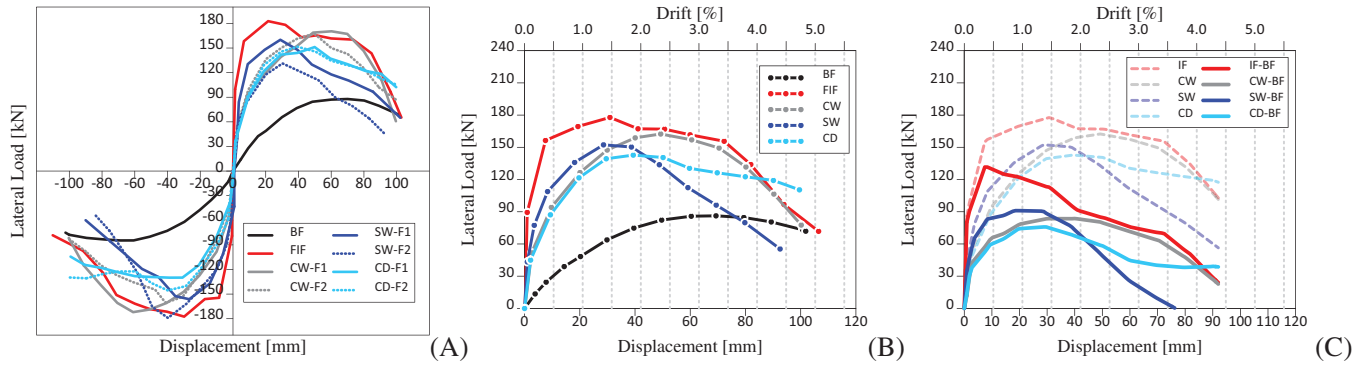


FIGURE 11 Envelope curves: (A) positive and negative envelopes; (B) average envelopes; (C) average envelopes of the infilled frames subtracted of the bare frame contribution.

TABLE 5 Initial stiffness and initial stiffness ratios of the specimens.

Specimen	K_0 (kN/mm)	$K_0/K_{B,0}$ (-)	K_0/K_{FI} (-)
BF	3.3	—	—
FIF	70.8	21.25	1.00
CW-F1/2	17.6	5.28	0.25
SW-F1/2	21.0	6.30	0.30
DW-F1/2	19.6	5.87	0.28

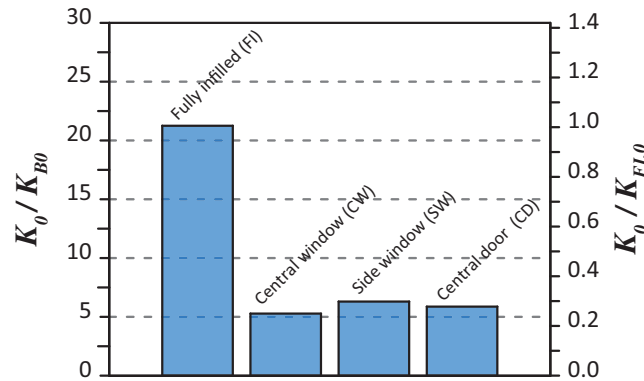


FIGURE 12 Initial stiffness ratios of the infilled frames with respect to the bare frame and the fully infilled frame.

On the other hand, the fully infilled frame had a stronger stiffness decay at very low drifts. From Figure 13A it can be observed that the secant stiffness of the FIF at 0.5% drift was about 20% of the initial one, while the infilled frames with the openings were subjected to a stiffness reduction of about 50% for the same drift level. Figure 13A also shows that the stiffness reduction trend of infilled frame specimens with openings was intermediate between the bare frame and the fully infilled frame. The secant stiffness trend of the specimens is compared in Figure 13B,C. The latter are normalized by the secant stiffness of the bare frame (K_B) and of the fully infilled frame (K_{FI}), respectively. It can be observed that in correspondence with drifts larger than 1.2%, the stiffness of the CW and CD specimens was similar to that of the FIF. In this drift interval, the stiffness increment with respect to the bare frame (K/K_B) was limited in a range varying from 2.7 to 1.5. A different trend was followed by the infilled frames with eccentric openings (SW), showing a significant loss of stiffness after 2% drift, which is consistent with a major damage accumulation. Similar considerations can be drawn by observing the trends in Figure 13C, where the stiffness reduction of the SW specimens after 2% drift results are more evident. As regards the CD specimens, the sudden increase of the ratio K/K_{FI} after 4% drift denotes a larger ductility even with very high drifts.

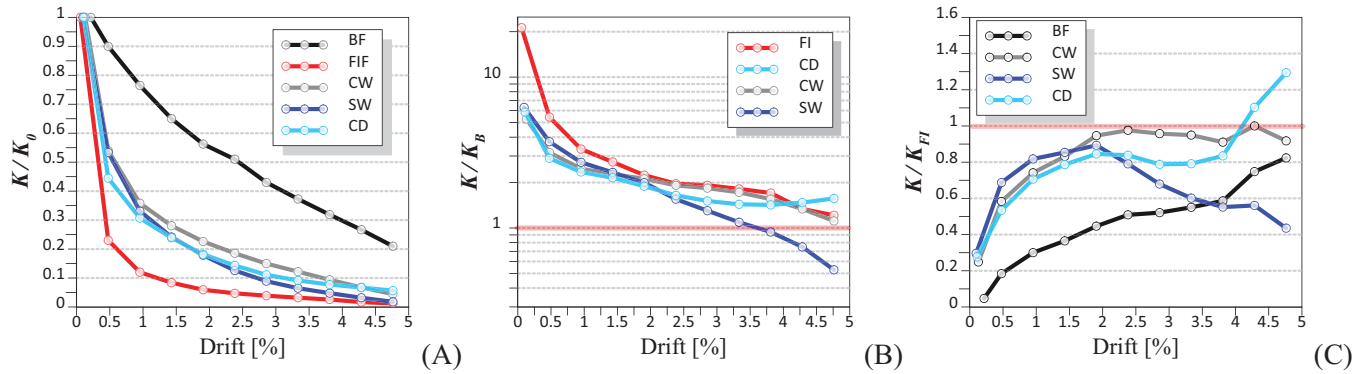


FIGURE 13 Secant stiffness ratios at the different drift levels: (A) K/K_0 ; (B) K/K_B ; (C) K/K_{FI} .

TABLE 6 Peak and ultimate resistances and displacements of the specimens.

Specimen	R_{peak} (kN)	$R_{peak}/R_{B,peak}$ (—)	$R_{peak}/R_{FI,peak}$ (—)	R_{ult} (kN)	d_{peak}	$d_{r,peak}$ (%)	$d_{peak}/d_{B,peak}$ (—)	$d_{peak}/d_{FI,peak}$ (—)	d_{ult} (mm)	$d_{r,ult}$ (%)	$d_{ult}/d_{B,ult}$ (—)	$d_{ult}/d_{FI,ult}$ (—)
BF	86	1.00	—	73.1	60.0	2.86%	1.00	—	100	4.76%	1.00	—
FIF	178	2.07	1.00	151.3	31.0	1.48%	0.52	1.00	73	3.48%	0.73	1.00
CW-F1/2	163	1.90	0.92	138.6	49.0	2.33%	0.82	1.58	76	3.62%	0.76	1.04
SW-F1/2	152	1.77	0.85	129.2	28.0	1.33%	0.47	0.90	51	2.43%	0.51	0.70
DW-F1/2	142	1.65	0.80	120.7	40.0	1.90%	0.67	1.29	90	4.29%	0.90	1.23

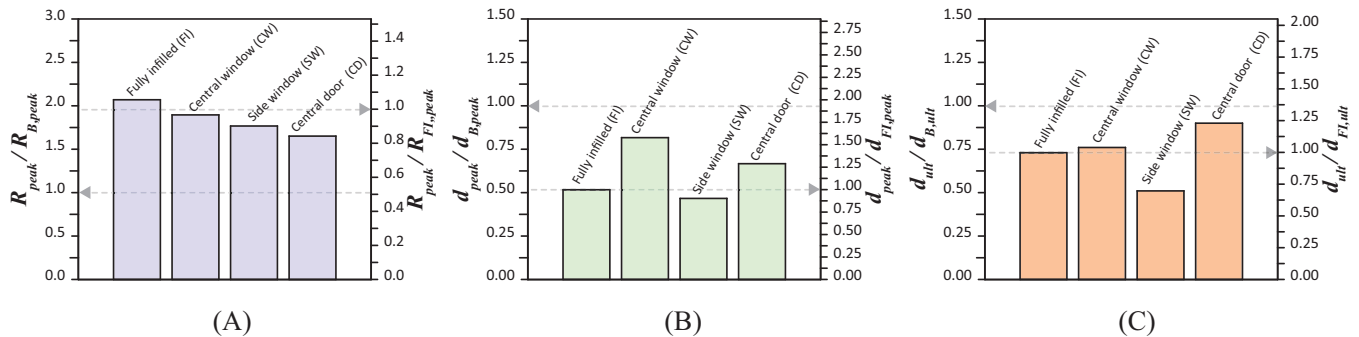


FIGURE 14 Resistance and displacement ratios of the infilled frames with respect to the bare frame and the fully infilled: (A) peak resistance; (B) peak displacements; (C) ultimate displacements.

Table 6 reports the peak resistances (R_{peak}), displacements (d_{peak}), interstorey drifts ($d_{r,peak}$), ultimate resistances (R_{ult}), displacements (d_{ult}) and drifts ($d_{r,ult}$) of the specimens. The ultimate displacements are evaluated as those associated with an 85% reduction of the peak resistance. Table 6 also reports resistance and displacement ratios with respect to the bare frame and the fully infilled frame. As regards the peak resistance, the fully infilled frame showed an increase of about two times that of the bare frame. The peak resistance was achieved at 1.48% drift, which is about half of the peak drift of the bare frame. The peak resistances of the infilled frames with the openings did not show a significant reduction, ranging between 80% and 92% the FIF peak resistance (Figure 14A). However, some relevant differences can be recognized in terms of peak and ultimate drifts. In fact, from Table 6 and Figure 14B, it can be observed that the specimens with central openings, CW and DW, had a shifting of the peak drifts by +58% and +29% respectively, with respect to the FIF. On the contrary, a reduction of the peak drift by −10% was observed for the specimens with eccentric openings (SW). As regards the ultimate drifts, the FIF achieved an ultimate drift of 3.48%, namely 73% of that of the BF. The infilled frames with openings showed significantly different post-peak trends (Figure 14C). In fact, while the CW specimens had an ultimate drift (3.62%) similar to that of the FIF, the CD specimens showed an increase of 23%. On the contrary, the SW specimens had a 30% reduction of the ultimate drift with respect to the FIF, denoting a more brittle behavior. The above-referred considerations can be also

recognized from Figure 11C, showing the contribution of the infills only, which is obtained by subtracting the bare frame response from the overall responses of the infilled frames.

Based on the experimental data, several conclusions can be drawn. Firstly, it appears that infilled frames with openings may be capable of developing alternative mechanisms for resisting loading, thus achieving peak resistances comparable to the fully infilled frames. Secondly, the peak and ultimate drifts of infilled frames with openings exhibit substantial variations depending on the opening arrangement. Specifically, central openings appear to have the effect of shifting the peak and ultimate drifts in comparison to fully infilled frames, with central door specimens displaying a particularly ductile behavior. In contrast, infilled frames with eccentric windows exhibited an earlier onset of peak response and a steeper post-peak slope, indicating a more severe damage (SD) accumulation.

3.2 | Energy dissipation

The energy dissipation was assessed by evaluating different energy-related parameters, namely the energy dissipation per cycle (W_d), the cumulative energy dissipation (ΣW_d), and the average energy dissipation per unit length ($W_d/2\delta$). The latter was obtained by dividing the energy dissipation per cycle by the total peak-to-peak displacement variation for each cycle (2δ). Results are illustrated in Figure 15. All the infilled frame specimens dissipated far more energy than the bare frame at each cycle (Figure 15A), independently from the presence of the openings. Moreover, the first cycle of three repeated is characterized by large dissipation indicating degradation of the mechanical behavior (Figure 10). However, significantly different energy dissipation trends have been observed in the different cases. The fully infilled frame dissipated more than all the other specimens up to 1.5% interstorey drift (Figure 15A,B). The average energy dissipation per unit length of the FIF, was quite high at the lower drifts, but rapidly decreased up to 2% drift (Figure 15B). Beyond this drift, $W_d/2\delta$ stabilized to constant value. Infilled frame specimens with central window and door openings showed a much more stable trend. For these specimens, the average energy dissipation per unit length was initially significantly lower than the FI specimen, but it remained approximately constant from 1 to 3.5% drift. In this range, the CW specimen showed approximately double energy dissipation capacity of the CD. This is also evident in terms of cumulative energy dissipation (Figure 15C). It is also noteworthy to observe that beyond 1.5% drift, the CW specimen dissipated more energy than the FIF (Figure 15B). A different response was recognized from the specimen with the eccentric window (SW). The latter had a similar energy dissipation capacity to the CW specimen up to 1.5% drift (Figure 15B). Beyond this point, the energy dissipation constantly decreased. Finally, observing cumulative energy dissipation curves in Figure 15B, and considering the average monotonic envelopes shown in Figure 10B, it can be generally noted that specimens having a higher stiffness (FI and SW), and so subjected to earlier damage, showed also higher energy dissipation at the lower drifts, while this was reduced when the displacement demand increased. Conversely, specimens having lower initial stiffness (CW and CD), showed a stable energy dissipation capacity, that was maintained even in correspondence with high drift demands.

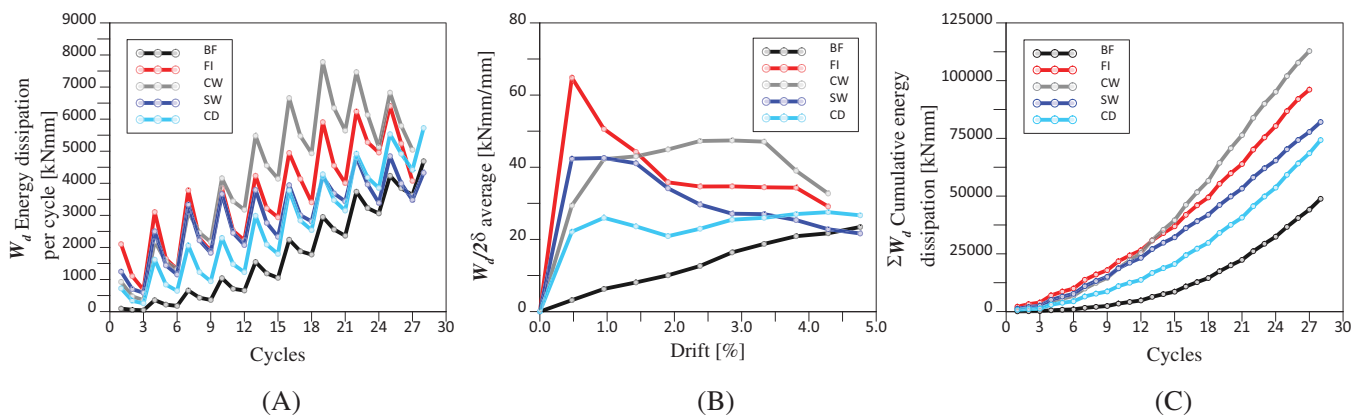


FIGURE 15 Energy dissipation: (A) energy dissipation per cycle; (B) average energy dissipation per unit length; (C) cumulative energy dissipation.

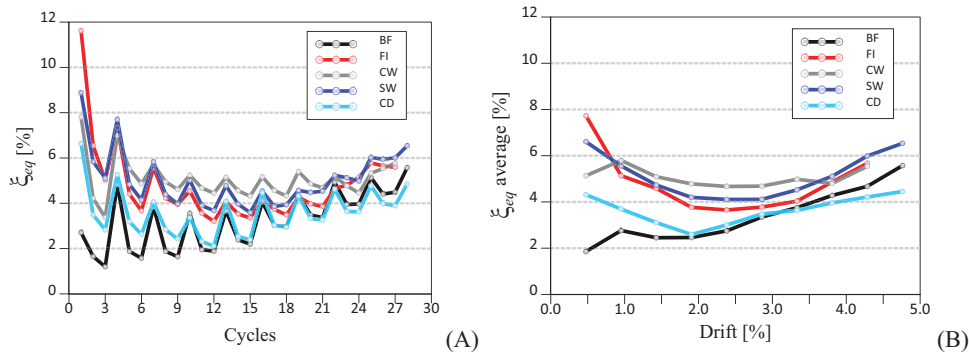


FIGURE 16 Equivalent viscous damping: (A) equivalent viscous damping per cycle; (B) average equivalent viscous damping at different drifts.

The equivalent viscous damping (ξ_{eq}) at the different cycles was also evaluated as:

$$\xi_{eq} = \frac{W_d}{2\pi(|W_e^+| + |W_e^-|)} \quad (1)$$

where W_d is the dissipated energy per cycle, and W_e^+ and W_e^- are the elastic energy at the positive and negative peak displacements, respectively. Results for each cycle are illustrated in Figure 16A, while the average ξ_{eq} values per cycle are reported in Figure 16B as a function of the interstorey drifts. The data presented in Figure 16 demonstrate that while the bare frame experienced a steady increase in between 2% and 6% drifts, the infilled frame exhibited a distinct behavior. As a matter of fact, ξ_{eq} values evaluated for the infilled frames showed a trend characterized by a first decrease up to 2%–2.5% drifts, followed by an increase at higher drift levels. The average values of ξ_{eq} for the FI, CW, and SW specimens were relatively similar at equivalent drift levels, primarily falling between 3.8% and 6%, while the CD specimen exhibited lower values in the range of 2.5%–4.5%.

4 | DAMAGE ANALYSIS

The infilled frame specimens exhibited distinct patterns of damage, as a function of the type and position of the openings. Through the examination of the test results, specific damage mechanisms were identified for each specimen. These mechanisms are further discussed below to provide a more detailed understanding of the variations in strength, stiffness, and energy dissipation capacity that were previously observed.

4.1 | Fully infilled frame specimen (FIF)

The test results inspection revealed that the initial light cracking of the infill and its separation from the surrounding frame occurred relatively early, at a drift level of 0.62%. The peak resistance was reached at 1.48% drift (Figure 17A). The damage pattern showed diagonal-stepped cracks due to the mortar joints sliding, without any significant damage to the bricks. This sliding mechanism persisted through large drift levels, resulting in the formation of alternative sliding crack patterns. This behavior is consistent with the ability of the specimen to maintain good energy dissipation capacity, as it does not exhibit significant post-peak resistance losses. The collapse displacement was reached at approximately 3.5%, where the largest strength reduction was recognized. The damage pattern at collapse showed extensive sliding of mortar joints, as well as localized crushing of the bricks at the upper-right corners and the middle of the infill (Figure 17B). Additionally, moderate shear and flexural cracks were identified at the mid-height and at the top of the columns. These observations allow singling out four main compression stress field characterizing the damage mechanism (Figure 17B).

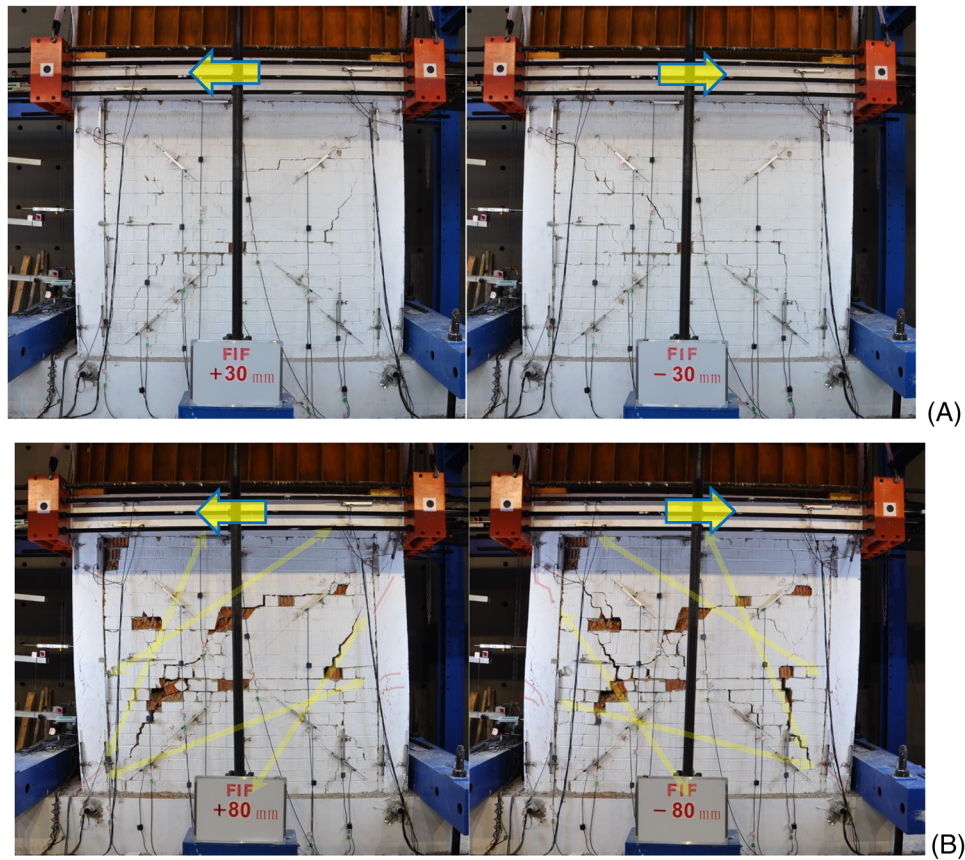


FIGURE 17 Damage patterns for the FIF specimen (positive and negative pushing): (A) at peak displacement; (B) at collapse.

4.2 | Central window specimens (CW)

The initial light damage of the infill was delayed with respect to the FIF, occurring at approximately 0.95% drift. The damage pattern up to the peak resistance (2.33% drift) (Figure 18A) showed combined flexural and shear cracks, alternatively affecting the portions of masonry at the left and at the right of the openings when the specimen was pushed in the positive and the negative direction. Beyond the peak displacement, a progressive reduction of resistance was recognized. The latter was associated with the increase of the shear damage, accompanied by wider cracks. The collapse drift (3.62%) was similar to that of the FIF. However, the damage at collapse (Figure 18B) was mainly localized on the portions of masonry at the left and the right of the opening. The initiation of shear cracks at the mid-height of the columns highlights that the main compression stress fields pass around the central opening (Figure 18B), producing a shifting of the shear demand along the columns. The presence of the central opening showed to affect more the stiffness than the resistance and the energy dissipation capacity, highlighting the effectiveness of the damage mechanism alternatively developed.

4.3 | Side window specimens (SW)

The initial damage of the infill occurred at about 0.48% drift. The damage mechanism was quite different with respect to the case with the central openings. The portion of the wall at the right of the opening resulted quite squat and stiff, polarizing a large amount of the lateral force. This resulted also in an earlier achievement of the peak displacement at 1.33% drift, which is significantly less than the CW (2.33%), and similar to the FIF (1.48%). The damage pattern up to the peak displacement (Figure 19A) already showed significant shear cracks concentrated in the masonry pier at the right of the opening, while no significant damage affected the remaining parts of the infill and of the frame. After the peak displacement, a rapid loss of strength was observed. The latter was associated with progressive damage of the right masonry pier, characterized by

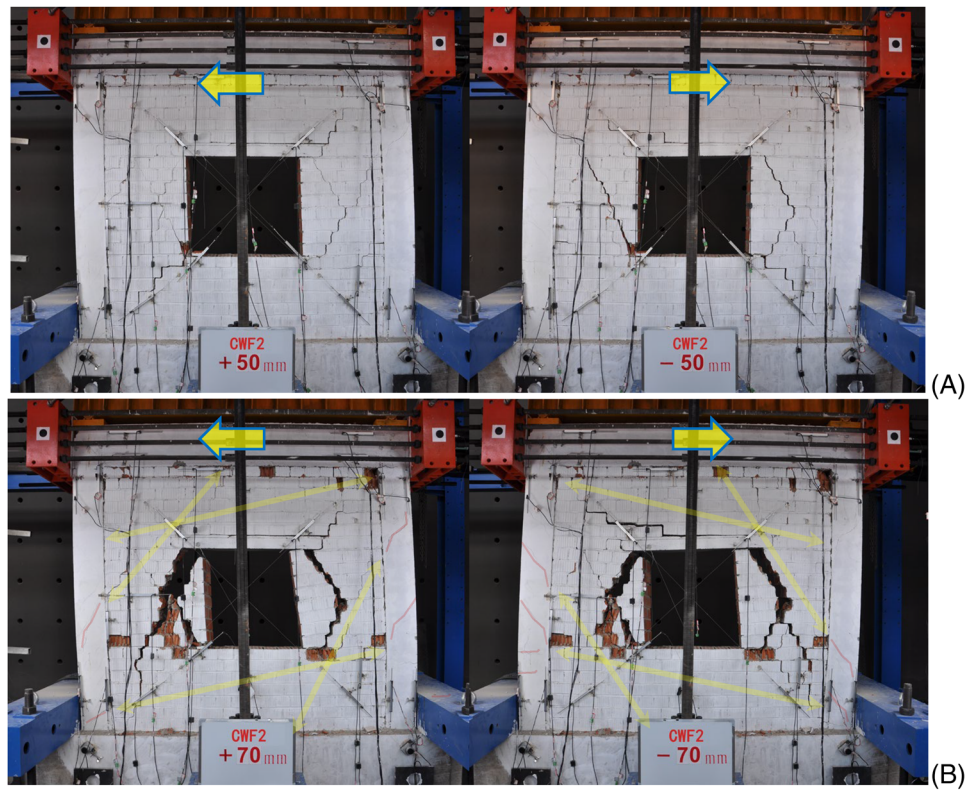


FIGURE 18 Damage pattern for the CW specimen (positive and negative pushing): (A) at peak displacement; (B) at collapse.

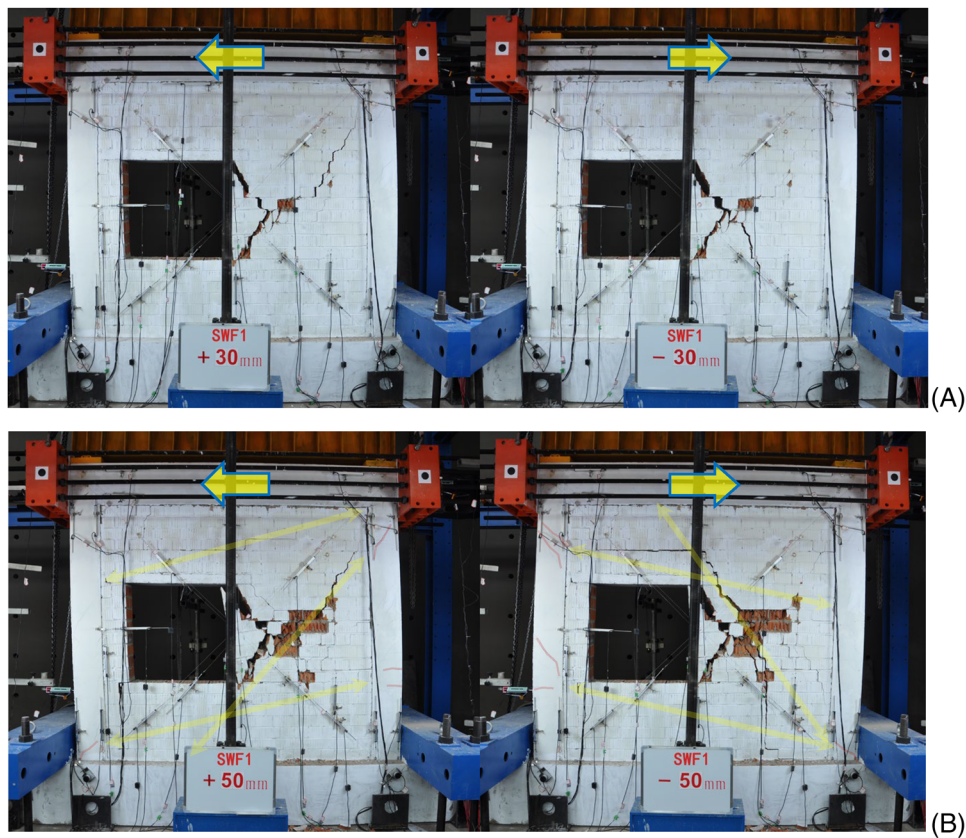


FIGURE 19 Damage pattern for the CW specimen (positive and negative pushing): (A) at peak resistance; (B) at collapse.

diffuse crushing of the bricks up to the collapse, which was achieved at 2.43% drift (Figure 19B). The examination of the test results revealed the presence of moderate cracks on the frame at the top and bottom of the columns. Additionally, flexural cracks were observed at approximately one-third of the height of both the left and right columns. Some initial signs of shear damage were also identified at the mid-height of the left column, which suggests the potential activation of a short column mechanism. The damage observed on the frame and infill is consistent with the main compression stress fields depicted in Figure 19B.

4.4 | Central door (CD)

The initial damage on the infill was significantly delayed with respect to the other specimens, occurring at about 1.33% drift. The observed damage mechanism was essentially flexural because of the pronounced slenderness of the masonry piers at the left and at the right of the door opening. The peak resistance was achieved at 1.90% drift. The peak damage pattern (Figure 20A) was characterized by flexural cracks crossing the mortar joints at the top and at the bottom of the masonry piers, evidencing a rocking behavior. The post-peak response was characterized by an amplification of the rocking mechanism, with a moderate increase of damage and a slight reduction of resistance denoting a pronounced ductile behavior. The collapse occurred at a very high drift (4.52%). The damage pattern showed localized crushing of the bricks at the base of the masonry piers and at the bottom of the beam (Figure 20B). Moderate shear cracks were recognized on the frame at the top of the columns and also in their central portion. The latter, as well as the damage on the infill, are consistent with the compression stress fields illustrated in Figure 20B.

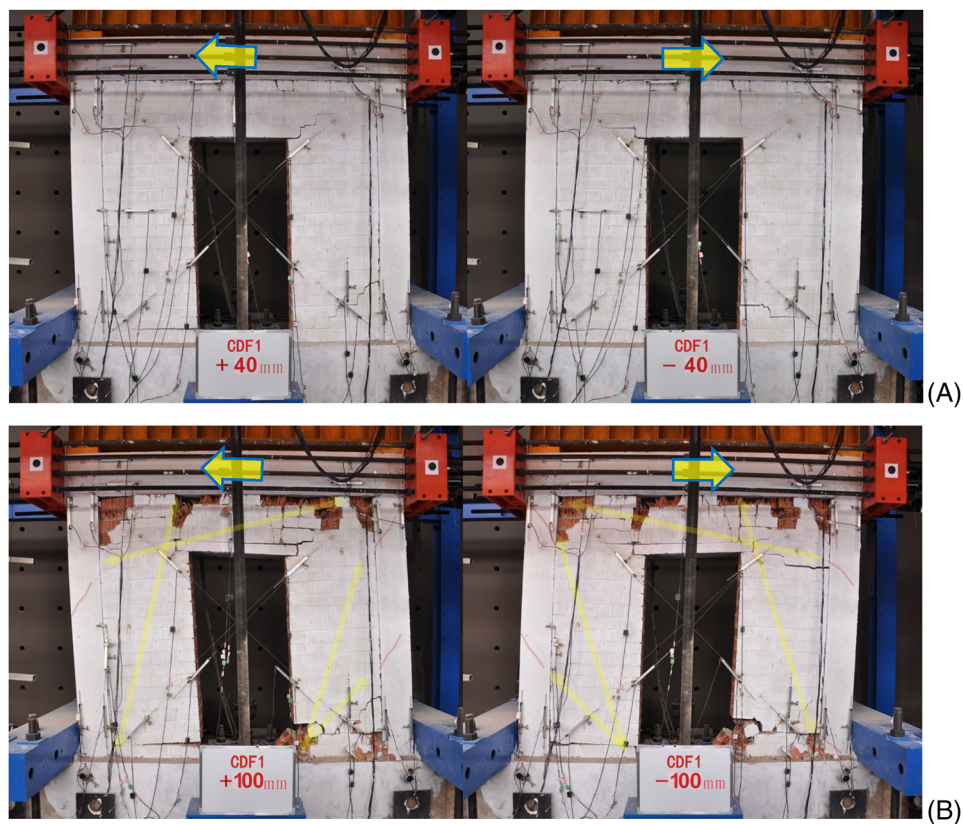


FIGURE 20 Damage pattern for the CD specimen (positive and negative pushing): (A) at peak resistance; (B) at collapse.

4.5 | Individuation of the limit states thresholds

The definition of damage-based reference limit states for reinforced concrete infilled frames has been provided by different authors (e.g., Morandi et al.,⁴³ Cardone and Perrone,⁵⁸ Chiozzi and Miranda,⁵⁹ Di Trapani et al.⁶⁰), although the proposed

drift limits are conflicting in some cases, as it is common with observational metrics. Three reference limit states have been identified to classify the observed damage states: damage limitation (DL), SD, and collapse prevention (CP).

The DL limit state was determined when the masonry infill detached from the frame, resulting in the formation of light cracks along the infill-frame interface. Additionally, diagonal light cracking of the mortar joints was observed, while no significant damage was identified on the bricks or the frame. At this damage level, the infill could typically be repaired through localized plastering and painting without significant structural implications.

The SD limit state was characterized by the formation of additional larger cracks along the mortar joints and bricks. Localized crushing of the bricks was also observed (such as at the corners or in the middle of the infills), and moderate cracks were also identified crossing the frame members. At this damage level, the out-of-plane stability of the infill was partially compromised. The infill could be repaired through reinforcement interventions, such as the application of a reinforced plaster, after the replacement of the crushed bricks.

The CP limit state was reached when the infill experienced an advanced damage state. This was characterized by the presence of large cracks crossing the infill, extensive crushing of the bricks, and in some cases, partial or total collapse of portions of the masonry. Cracks were also clear in the frame members, and the out-of-plane stability of the infill was significantly compromised. At this damage level, replacement of the infill would be more appropriate than attempting to repair it.

Reference pictures of the damage patterns associated with the achievement of each limit states for the infilled frame specimens are illustrated in Figure 21.

The interstorey drifts associated with the achievement of the different limit states for the specimens are reported in Table 7. In Figure 22, the recognized limit state thresholds are reported on the average envelope curves. The presence, type, and position of the openings have a significant impact on the drift at which the limit states occur. In general, it can be observed that the specimens with an eccentric opening achieved the limit state thresholds at significantly earlier drifts compared to the fully infilled frame. Conversely, the CD specimen showed a noticeable delay of all the damage thresholds. An intermediate trend was observed for the CW specimen, showing a delay of the DL and anticipation of SD and CP limit states. It is not possible to generalize about the interstorey drifts associated with the different limit states. However, the general trend outlined in this study indicates that masonry infills with openings realized in such a way to form slender masonry piers at the sides undergo a delay of damage because of the activation of a flexural, or mixed flexural-shear, mechanism. Conversely, if the openings form squat masonry piers at their sides, the achievement of the limit state thresholds will occur earlier due to a greater susceptibility to shear damage. The geometrical arrangement of the openings plays a critical role in this context.

5 | EMPIRICAL ANALYSIS OF THE PEAK RESPONSE OF INFILLED FRAMES WITH OPENINGS

The experimental results from this and previous studies have consistently shown that the response of infilled frames is greatly influenced by the type and position of the openings. As previously discussed, masonry infills with openings may develop alternative mechanisms for resisting lateral loads. In general, an increase in the opening ratio was found to be associated with a decrease in initial stiffness, peak resistance, and a forward shift of the peak displacement. Table 8 collects data from 34 experimental tests on infilled frames with window and door openings by 8 experimental studies (including the current one), and that of the respective fully infilled frames. Response parameters collected refer to the experimental averages of peak force and displacement values from the positive and negative envelopes. The latter are the average peak resistances (R_{peak}) and the average peak interstorey drifts ($d_{r,peak}$). Additionally, the ratios $R_{peak}/R_{FI,peak}$ and $d_{r,peak}/d_{rFI,peak}$ were evaluated. They represent the previously defined parameters normalized by the same evaluated for the respective fully infilled frame. Finally, the peak strength reduction factor with respect to that of the fully infilled frame (r) was evaluated as:

$$r = \frac{\Delta R_{peak}}{\Delta R_{FI,peak}} = \frac{R_{peak} - R_{BF,peak}}{R_{FI,peak} - R_{BF,peak}} \quad (2)$$

where $R_{BF,peak}$ is the peak resistance of the bare frame. Table 8 also reports the geometric ratios A_o/A_i , l_o/l_i and h_o/h_i characterizing the openings for the different specimens. The dataset presented in Table 8 has been used to study the

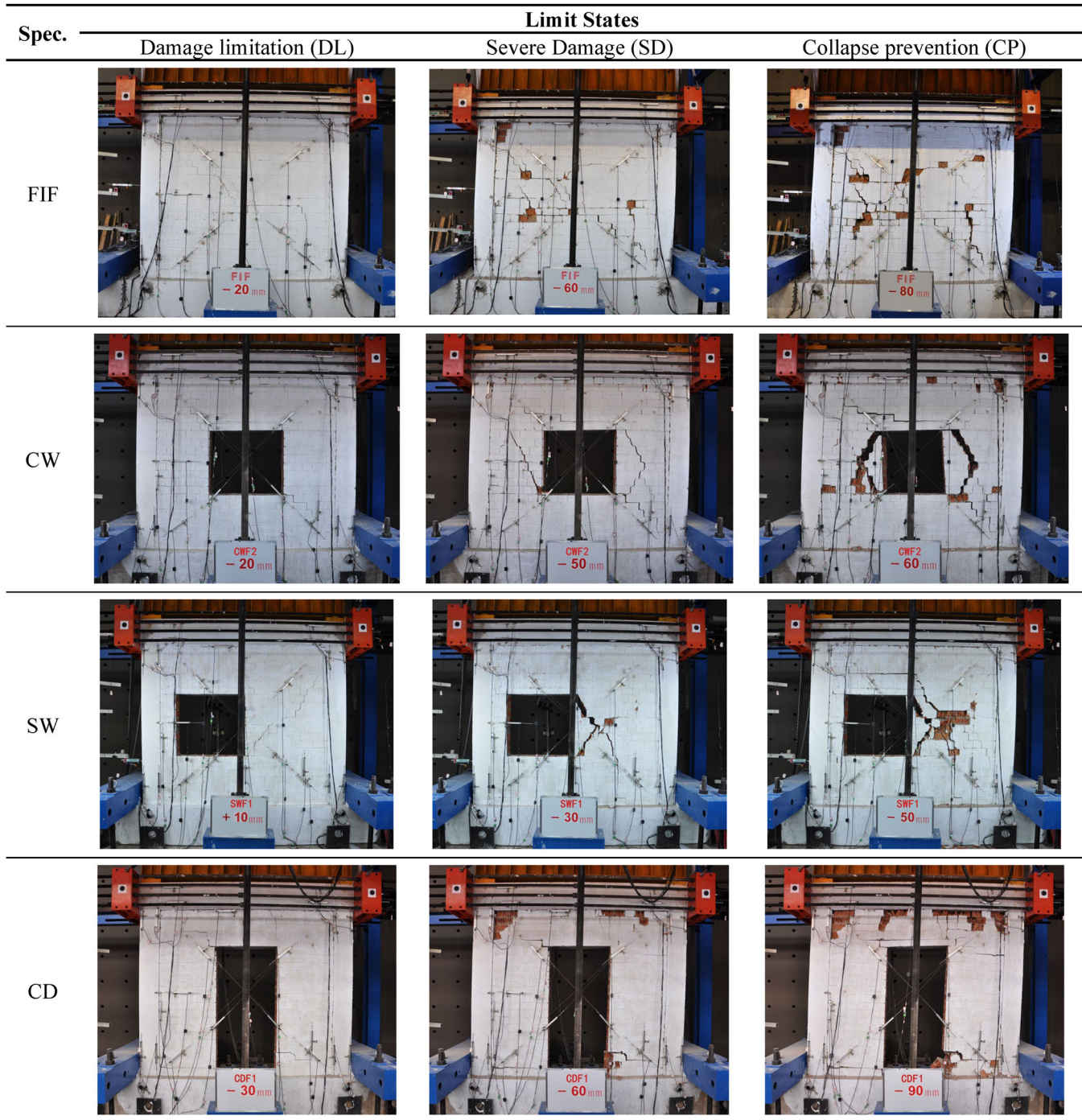


FIGURE 21 Damage patterns associated with the limit states for the infilled frame specimens.

TABLE 7 Percentage drift associated with the limit states for the specimens.

Specimen	$d_{r,DL}$ (%)	$d_{r,SD}$ (%)	$d_{r,CP}$ (%)
FIF	0.62%	2.62%	3.76%
CW-F1/2	0.95%	2.14%	2.86%
SW-F1/2	0.48%	1.19%	2.14%
DW-F1/2	1.33%	2.86%	4.29%

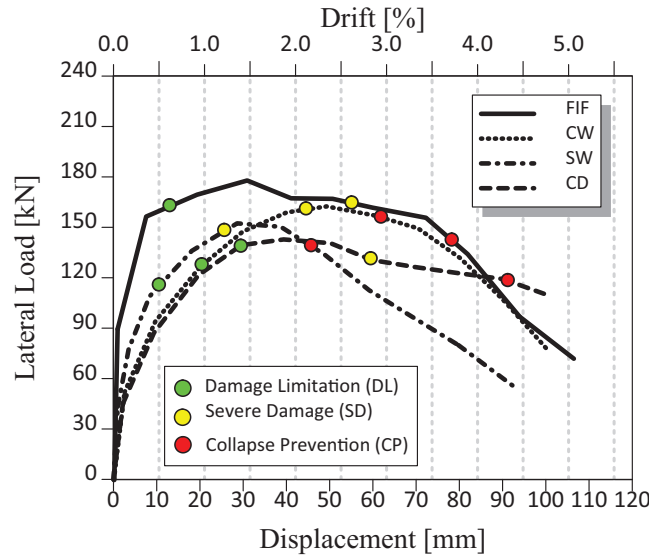


FIGURE 22 Limit states identified on the average envelopes.

correlations between the geometry arrangement of the openings and the expected modification of the peak response parameters.

Data from specimens with window and door openings have been analyzed separately. Correlations were aimed at the estimation of both the peak strength reduction factor (r) and the peak drift increment factor ($d_{peak}/d_{IF,peak}$). Two different estimators (A and B) were defined to correlate the geometric parameters A_o/A_i , l_o/l_i and h_o/h_i to the peak strength reduction factor of the infilled frames with the door and the window openings. The functionals of the estimators were defined by setting a nonlinear combination of the geometric parameters characterizing the openings in such a way to obtain the maximum possible determination coefficient of the regression model. The finally obtained estimators have the following form:

$$A = 1.5 \left(\frac{A_o}{A_i} \right)^{1.7} + 1.6 \left(\frac{l_o}{l_i} \right)^{1.7} \quad (3)$$

$$B = \left(\frac{A_o}{A_i} \right)^2 + 0.5 \left(\frac{h_o}{h_i} \right)^2 \quad (4)$$

It was found that in both cases the overall opening ratio (A_o/A_i) played a major influence on the reduction of the peak resistance. However, because of the different lateral resisting mechanisms activated in the cases of the window or door openings, the strongest correlations were found combining A_o/A_i with the horizontal opening ratio (l_o/l_i) and the vertical opening ratio (h_o/h_i), for infills with window and door openings respectively (Figure 23A,B). Infills with windows mainly involved damage to the masonry piers at the sides of the opening. In this framework, the horizontal opening ratio (l_o/l_i) provided an effective measure of the available transverse resisting area of the infill. With regards to infills with doors, the resisting mechanism still relied on the masonry piers at the sides of the opening, however, the lateral resisting capacity provided by the infill was substantially affected by the degree of coupling of the piers, which was ensured by the lintel above the door. Therefore, considering the vertical opening ratio (h_o/h_i), significantly improved correlation with the r factor. (Figure 23B). The regression models provided in Figure 23 are limited by the values $r = 1$.

The peak drift modification due to the presence of the openings was also analyzed. In this case the peak strength reduction factor r was assumed as estimator, as this parameter can effectively summarize the effect of the opening size, typology, and position (Figure 24A,B). It could be generally recognized that the infilled frames with openings were subjected to a major increase in peak drift when the net resistance ratio decreased because of the openings. The analytical expression used to fit data in Figures 23 and 24 are here used to provide a rough estimation of the overall trend. A more robust analysis of data would be desirable to provide more accurate predictive equations.

TABLE 8 Peak response parameters and geometric opening ratios from previous and current studies.

Reference	Specimen	Scale	Opening type	Opening position	Type of masonry	A_o/A_i (—)	l_o/l_i (—)	h_t/h_i (—)	R_{peak} (kN)	$R_{peak}/R_{FI,peak}$ (—)	$\Delta R_{peak}/\Delta R_{FI,peak}$ (—)	$d_{r,peak}$ (%)	$d_{r,peak}/d_{r,FI,peak}$ (—)
Basha et al. ⁴⁴	IF-A _r -0	1:2	N	—	Fly ash bricks	—	—	—	106	1.00	1.00	0.45	1.00
	IF-A _r -10	1:2	W	C	Fly ash bricks	0.10	0.32	0.34	73.5	0.69	0.52	1.50	3.33
	IF-A _r -20	1:2	W	C	Fly ash bricks	0.20	0.45	0.28	75.5	0.71	0.55	1.20	2.67
	IF-A _r -30	1:2	W	C	Fly ash bricks	0.30	0.55	0.23	54	0.51	0.24	1.60	3.56
	IF-A _r -40	1:2	W	C	Fly ash bricks	0.40	0.63	0.18	51	0.48	0.19	1.60	3.56
	IF-A _r -50	1:2	W	C	Fly ash bricks	0.50	0.71	0.15	54.5	0.51	0.24	1.75	3.89
Sigmund and Penava ⁴⁰	III/2	1:2.5	N	—	Hollow clay bricks	0.00	0.00	0.00	275	1.00	1.00	—	—
	I/1	1:2.5	D	C	Hollow clay bricks	0.15	0.22	0.31	300	1.09	0.42	—	—
	I/2	1:2.5	W	C	Hollow clay bricks	0.14	0.31	0.23	255	0.93	0.23	—	—
	I/3	1:2.5	D	E	Hollow clay bricks	0.15	0.22	0.31	266	0.97	0.28	—	—
	I/4	1:2.5	W	E	Hollow clay bricks	0.14	0.31	0.23	255	0.93	0.23	—	—
	S	1:2	N	—	Clay bricks	0.00	0.00	0.00	116.3	1.00	1.00	—	—
Mansouri et al. ⁴²	DO	1:2	D	C	Clay bricks	0.16	0.21	0.23	82.3	0.71	0.30	—	—
	RWO	1:2	W	C	Clay bricks	0.16	0.36	0.12	90.5	0.78	0.47	—	—
	LWO	1:2	W	C	Clay bricks	0.27	0.48	0.12	84.3	0.72	0.34	—	—
	EWO	1:2	W	E	Clay bricks	0.16	0.36	0.12	89.5	0.77	0.45	—	—
	2	1:1	N	—	Hollow conc blocks	0.00	0.00	0.00	305	1.00	1.00	0.60	1.00
	3	1:1	W	C	Hollow conc blocks	0.20	0.43	0.23	240	0.79	0.32	1.60	2.67
Zhai et al. ⁴¹	4	1:1	W	C	Hollow conc blocks	0.19	0.42	0.23	290	0.95	0.84	1.40	2.33
	TA2	1:1	N	—	Hollow clay units	0.29	0.00	0.00	550	1.00	1.00	—	—
	TA4	1:1	D	C	Hollow clay units	0.29	0.29	0.00	306	1.00	0.02	—	—
Morandi et al. ¹¹	SW	2:3	W	E	Clay bricks	0.12	0.29	0.27	605	0.92	0.89	0.41	1.58
	DO	2:3	D	E	Clay bricks	0.16	0.21	0.24	487.5	0.74	0.66	0.60	2.31
	Blackard et al. ³⁹	2:3	N	—	Clay bricks	0.00	0.00	0.00	660	1.00	1.00	0.26	1.00

(Continues)

TABLE 8 (Continued)

Reference	Specimen	Scale	Opening type	Opening position	Type of masonry	A_0/A_i (—)	l_0/l_i (—)	h_i/h_i (—)	R_{peak} (kN)	$R_{peak}/R_{FI,peak}$ (—)	$\Delta R_{peak}/\Delta R_{FI,peak}$ (—)	$d_{r,peak}$ (%)	$d_{r,peak}/d_{r,FI,peak}$ (—)
Kakaletsis and Karayannis ^{36–38}	S	1:3	N	—	Clay bricks	0.00	0.00	0.00	78	1.00	1.00	0.75	1.00
	WO2	1:3	W	C	Clay bricks	0.11	0.25	0.19	66.5	0.85	0.68	1.04	1.39
	WO3	1:3	W	C	Clay bricks	0.15	0.33	0.19	69	0.88	0.75	1.08	1.44
	WO4	1:3	W	C	Clay bricks	0.20	0.46	0.19	63.5	0.81	0.60	1.08	1.44
	DO2	1:3	D	C	Clay bricks	0.20	0.25	0.19	56	0.72	0.39	1.13	1.50
	DO3	1:3	D	C	Clay bricks	0.27	0.33	0.19	57	0.73	0.42	0.96	1.28
	DO4	1:3	D	C	Clay bricks	0.37	0.46	0.19	51	0.65	0.25	1.54	2.06
	WX1	1:3	W	E	Clay bricks	0.11	0.25	0.19	71	0.91	0.81	1.50	2.00
	WX2	1:3	W	E	Clay bricks	0.11	0.25	0.19	69	0.88	0.75	1.33	1.78
	DX1	1:3	D	E	Clay bricks	0.20	0.25	0.19	58	0.74	0.44	1.33	1.78
	DX2	1:3	D	E	Clay bricks	0.20	0.25	0.19	62	0.79	0.56	1.00	1.33
	IS	1:3	N	—	Clay bricks	0.00	0.00	0.00	68.5	1.00	1.00	1.00	1.00
This study	IDO2	1:3	D	C	Clay bricks	0.20	0.25	0.19	57.5	0.84	0.43	0.92	0.92
	IWO2	1:3	W	C	Clay bricks	0.11	0.25	0.19	63	0.92	0.58	1.17	1.17
	IF	2:3	N	—	Hollow clay bricks	0.00	0.00	0.00	178	1.00	1.00	1.48	1.00
	CWF-1/2	2:3	W	C	Hollow clay bricks	0.16	0.41	0.31	163	0.92	0.84	2.33	1.57
	SWF-1/2	2:3	W	E	Hollow clay bricks	0.16	0.41	0.31	152	0.85	0.72	1.33	0.90
	CDF-1/2	2:3	D	C	Hollow clay bricks	0.27	0.34	0.21	142	0.80	0.61	1.90	1.28

Abbreviations: C, central; D, door; E, eccentric; N, none; W, window.

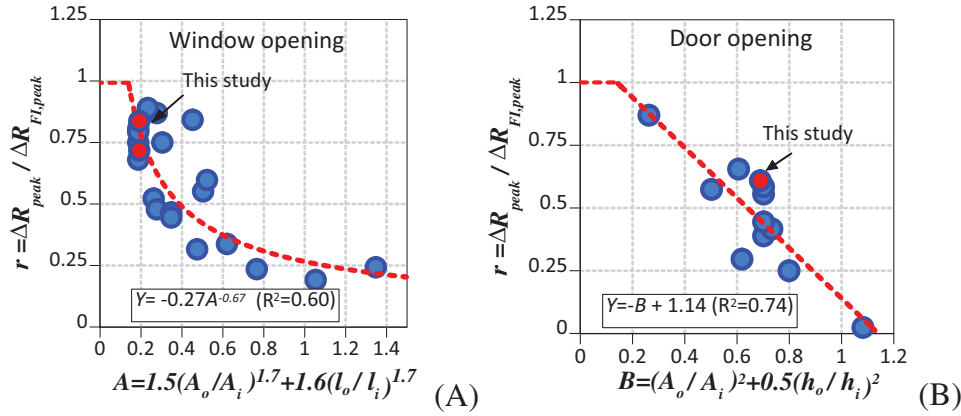


FIGURE 23 Peak resistance modification as a function of the opening ratio: (A) window openings; (B) door openings.

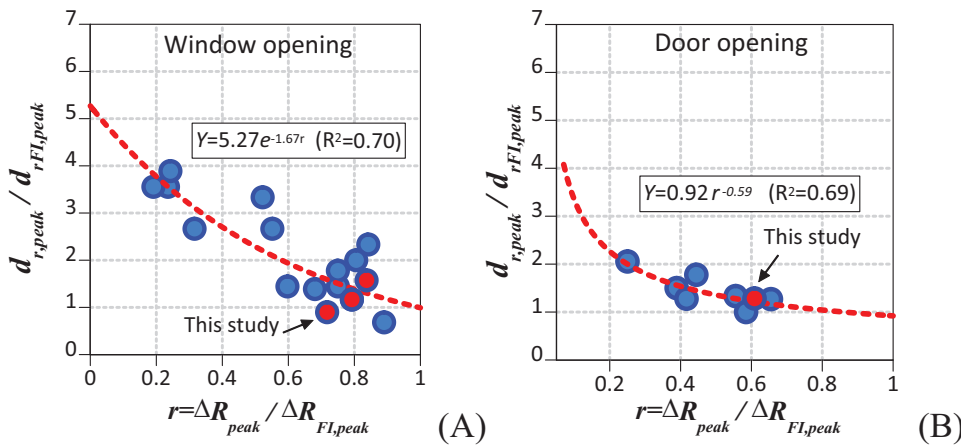


FIGURE 24 Peak drift modification as a function of the net resistance ratio: (A) window openings; (B) door openings.

6 | CONCLUSIONS

This paper presented the results of an experimental investigation involving seven 2/3 scale infilled frames constructed with hollow clay brick masonry and subjected to quasi-static cyclic lateral loading. The specimens included solid infills as well as infills with door and window openings, with central and eccentric configurations. The influence of the type and position of the openings on strength, stiffness, and energy dissipation capacity was analyzed. The damage mechanisms associated with each configuration were also studied, as well as the achievement of relevant limit states. Literature data regarding previous experimental tests on infilled frames with openings were collected and combined with the results of the current experimental campaign, to evaluate the dependence of the peak response on the opening arrangement of an infilled frame. Based on the obtained results, the following conclusions can be drawn:

1. Openings in masonry infills significantly modify the overall response with respect to the case of fully infilled frames. A strong infill-frame interaction is still recognized because of the development of alternative resisting mechanisms.
2. The tested infilled frames with openings had lower initial stiffness (-70%) with respect to that of the fully infilled frame. However, the initial stiffness of the infilled frames with openings was still 6 times higher than that of the bare frames. Infilled frames with openings had however a lower stiffness decay so their secant stiffness became similar to that of the fully infilled frames after 0.5% drift.
3. The opening typology and position conditioned the initial stiffness and the secant stiffness during the tests. Infills with eccentric openings were stiffer, but at the same time they suffered a significant post-peak stiffness decay. Infills with central door openings had lower initial stiffness but also showed reduced secant stiffness decay, even with high interstorey drifts. An intermediate behavior was observed in case of central window openings.

4. The peak resistances of the infilled frames with the opening ratios considered in this experimental campaign did not show significant reductions with respect to the fully infilled frame case. Their peak resistance ranged between 80% and 92% of the FIF peak resistance, meaning that alternative resisting mechanisms could develop despite the different geometrical arrangements.
5. Peak and ultimate drifts are substantially affected by the presence of openings. Specimens with central openings, CW and DW, showed a shifting of the peak drifts by +58% and +29% respectively, while the ultimate drifts were similar to that of the FIF. Conversely, a reduction of the peak drift by −10% and of the ultimate drift by −30% was recognized for the specimens with eccentric openings (SW), denoting that opening eccentricity may result in an anticipation of damage initiation and evolution.
6. Regardless of the location of the openings, all infilled frame specimens demonstrated a significantly higher energy dissipation capacity compared to the bare frame. Specifically, those with eccentric openings exhibited a higher dissipation rate during the initial cycles, while those with central openings displayed a more consistent dissipation capacity, even in the presence of significant drift.
7. The observed damage patterns have shown substantially different damage mechanism development as a function of the typology and position of the openings. It was recognized that masonry infills with openings realized in such a way to form slender masonry piers at the sides delayed the achievement of the damage thresholds because of the activation of a flexural, or mixed flexural-shear mechanism. On the contrary, openings forming squat masonry piers at their sides advanced the achievement of the limit state thresholds, because of larger propension to shear damage. In general, limit state drifts conventionally adopted for fully infilled frames are not valid in the case of infills with openings.
8. Some empirical expressions were used to fit data regarding the modification of the peak response as a function of the opening arrangement. The geometrical opening ratios showed to play a major role in the estimation of the peak response. However, a more robust regression analysis, including also mechanical variables would be desirable to arrive at more accurate predictive equations.

ACKNOWLEDGMENTS

The authors have nothing to report.

DATA AVAILABILITY STATEMENT

The data that support the findings of this study are available on request from the corresponding author. The data are not publicly available due to privacy or ethical restrictions.

ORCID

Fabio Di Trapani  <https://orcid.org/0000-0002-7578-0633>

Lin Zhou  <https://orcid.org/0000-0002-6018-4927>

REFERENCES

1. Huang H, Burton HV, Sattar S. Development and utilization of a database of infilled frame experiments for numerical modeling. *J Struct Eng*. 2020;146(6):04020079.
2. Mehrabi AB, Shing PB, Schuller MP, Noland L. Experimental evaluation of masonry-infilled RC frames. *J Struct*. 1996;122(3):228-237.
3. Calvi GM, Bolognini D. Seismic response of reinforced concrete frames infilled with weakly reinforced masonry panels. *J Earthq Eng*. 2001;5(02):153-185.
4. Al-Chaar G, Issa M, Sweeney S. Behavior of masonry-infilled nonductile reinforced concrete frames. *J Struct Eng*. 2002;128:1055-1063.
5. Papia M, Cavaleri L, Fossetti M. Infilled frames: developments in the evaluation of the stiffening effect of infills. *Struct Eng Mech*. 2003;16(6):675-693.
6. Colangelo F. Pseudo-dynamic seismic response of reinforced concrete frames infilled with non-structural brick masonry. *Earthq Eng Struct Dyn*. 2005;34:1219-1241.
7. da Porto F, Guidi M, Dalla Benetta N, Verlato F. Combined in-plane/out-of-plane experimental behaviour of reinforced and strengthened infill masonry walls. 12th Canadian Masonry Symposium; June 2–5, 2013. Vancouver, Canada.
8. Cavaleri L, Di Trapani F. Cyclic response of masonry infilled RC frames: experimental results and simplified modeling. *Soil Dyn Earthq Eng*. 2014;65:224-242.
9. Bergami A, Nuti C. Experimental tests and global modeling of masonry infilled frames. *Earthq Struct*. 2015;9(2):281-303.
10. Verderame GM, Ricci P, Del Gaudio C, De Risi MT. Experimental tests on masonry infilled gravity- and seismic-load designed RC frames. 16th international brick and block masonry conference, IBMAC 2016. 2016; 1349-1358.

11. Morandi P, Hak S, Magenes G. In-plane experimental response of strong masonry infills. *Eng Struct*. 2018;156:503-521.
12. Mehrabi AB, Shing PB. Finite element modelling of masonry-infilled RC frames. *J Struct Eng*. 1997;123(5):604-613.
13. Koutromanos I, Stavridis A, Shing PB, Willam K. Numerical modelling of masonry-infilled RC frames subjected to seismic loads. *Comput Struct*. 2011;89:1026-1037.
14. Calìo I, Pantò B. A macro-element modelling approach of infilled frame structures. *Comput Struct*. 2014;143:91-107.
15. Di Trapani F, Bertagnoli G, Ferrotto MF, Gino D. Empirical equations for the direct definition of stress-strain laws for fiber-section based macro-modeling of infilled frames. *J Eng Mech*. 2018;144(11):04018101.
16. Milanese RR, Morandi P, Magenes G. Local effects on RC frames induced by AAC masonry infills through FEM simulation of in-plane tests. *Bull of Earthq Eng*. 2018;16(1):4053-4080.
17. Di Trapani F, Giordano L, Mancini G. Progressive collapse response of reinforced concrete frame structures with masonry infills. *J Eng Mech*. 2020;146(3):04020002.
18. Bertoldi SH, Decanini LD, Gavarini C, Telai tamponati soggetti ad azioni sismiche, un modello semplificato: confronto sperimentale e numerico. Proceedings of the 6th Convegno Nazionale ANIDIS, 1993. Perugia, Italy.
19. Panagiotakos TB, Fardis MN. Seismic response of infilled RC frames structures. XXI WCEE 1966; Acapulco, Mexico.
20. Dolšek M, Fajfar P. The effect of masonry infills on the seismic response of four storey reinforced concrete frame—a deterministic assessment. *Eng Struct*. 2008;30(7):1991-2001.
21. Rodrigues H, Varum H, Costa A. Simplified macro-model for infill masonry panels. *J Earthq Eng*. 2010;14:390-416.
22. De Risi MT, Del Gaudio C, Ricci P, Verderame GM. In-plane behaviour and damage assessment of masonry infills with hollow clay bricks in RC frames. *Eng Struct*. 2018;168:257-275.
23. Liberatore L, Noto F, Mollaioli F, Franchin P. In-plane response of masonry infill walls: comprehensive experimentally based equivalent strut model for deterministic and probabilistic analysis. *Eng Struct*. 2018;167:533-548.
24. Di Trapani F. A novel data-driven force–displacement macro-model for nonlinear analysis of infilled frames: development, validation and reliability comparison. *Bull Earthq Eng*. 2021;19(14):6157-6186.
25. Chrysostomou CZ, Gergely P, Abel JF. A six-strut model for nonlinear dynamic analysis of steel infilled frames. *Int J Struct Stab Dyn*. 2002;02(3):335-353.
26. El-Dakhkhni W, Elgaaly M, Hamid A. Three-strut model for concrete masonry-infilled steel frames. *J Struct Eng*. 2003;129(2):177-185.
27. Crisafulli FJ, Carr AJ. Proposed macro-model for the analysis of infilled frame structures. *Bull NZ Soc Earthq Eng*. 2007;40:69-77.
28. Fiore A, Porco F, Raffaele D, Uva G. About the influence of the infill panels over the collapse mechanisms active under pushover analyses: two case studies. *Soil Dyn Earthq Eng*. 2012;39:11-22.
29. Jeon JS, Park JH, DesRoches R. Seismic fragility of lightly reinforced concrete frames with masonry infills. *Earthq Engng Struct Dyn*. 2015;44:1783-1803.
30. Di Trapani F, Tomaselli G, Cavaleri L, Bertagnoli G. Macroelement model for the progressive-collapse analysis of infilled frames. *J Struct Eng*. 2021;147(6):04021079.
31. Blasi G, De Luca F, Perrone D, Greco A, Aiello MA. MID 1.1: database for characterization of the lateral behavior of infilled frames. *J Struct Eng*. 2021;147(10):04721007.
32. Mohammadi M, Nikfar F. Strength and stiffness of masonry-infilled frames with central openings based on experimental results. *J Struct Eng*. 2013;139:974-984.
33. Dawe JL, Seah CK. Behaviour of masonry infilled steel frames. *Can J Civ Eng*. 1989;16(6):865-876.
34. Mosalam KM, White RN, Gergely P. Static response of infilled frames using quasi-static experimentation. *J Struct Eng*. 1997;123(11):1462-4169.
35. Tasnimi AA, Mohebbkhah A. Investigation on the behavior of brick-infilled steel frames with openings, experimental and analytical approaches. *Eng Struct*. 2011;33(3):968-980.
36. Kakaletsis DJ, Karayannis CG. Experimental investigation of infilled R/C frames with eccentric openings. *Struct Eng Mech*. 2007;26(3):231-250.
37. Kakaletsis DJ, Karayannis CG. Influence of masonry strength and openings on infilled R/C frames under cycling loading. *J Earthq Eng*. 2008;12(2):197-221.
38. Kakaletsis DJ, Karayannis CG. Experimental investigation of infilled reinforced concrete frames with openings. *ACI Struct J*. 2009;106(2):132-141.
39. Blackard B, Willam K, Mettupalayam S. Experimental observations of masonry infilled reinforced concrete frames with openings. *ACI Symposium Paper*. 2009;265:199-222.
40. Sigmund V, Penava D. Influence of openings, with and without confinement, on cyclic response of infilled R-C frames: an experimental study. *J Earthq Eng*. 2014;18(1):113-146.
41. Zhai C, Kong J, Wang X, Chen Z. Experimental and finite element analytical investigation of seismic behavior of full-scale masonry infilled RC frames. *J Earthq Eng*. 2016;20(7):1171-1198.
42. Mansouri A, Marefat MS, Khanmohammadi M. Experimental evaluation of seismic performance of low-shear strength masonry infills with openings in reinforced concrete frames with deficient seismic details. *Struct Des Tall Special Build*. 2014;23(15):1190-1210.
43. Morandi P, Hak S, Magenes G. Performance-based interpretation of in-plane cyclic tests on RC frames with strong masonry infills. *Eng Struct*. 2018;156:503-521.

44. Basha SH, Surendran S, Kaushik HB. Empirical models for lateral stiffness and strength of masonry-infilled RC frames considering the influence of openings. *J Struct Eng*. 2020;146(4):04020021.
45. Carvalho EC, Coelho E. Seismic assessment, strengthening and repair of structures. radECOEST2-ICONS report no. 2, European Q2 Commission—training and mobility of researchers programme. Laboratorio Nacional de Engenharia Civil, 2001; Lisboa, Portugal.
46. Al-Chaar G, Lamb GE, Issa M. Effect of openings on structural performance of unreinforced masonry infilled frames. *ACI Symposium Paper*. 2003;211:247-262.
47. Stavridis A, Koutromanos I, Shing PB. Shake-table tests of a three-story reinforced concrete frame with masonry infill walls. *Earthq Engng Struct Dyn*. 2011;41(6):1089-1108.
48. Durrani AJ, Luo YH. Seismic retrofit of flat-slab buildings with masonry infills. Proc., NCEER Workshop on Seismic Response of Masonry Infills, National Center for Earthquake Engineering Research, 1994; Buffalo, NY.
49. Asteris PG. Lateral stiffness of brick masonry infilled plane frames. *J Struct Eng*. 2003;129(8):1071-1079.
50. Mondal G, Jain SK. Lateral stiffness of masonry infilled reinforced concrete (RC) frames with central opening. *Earthq Spectra*. 2008;24(3):701-723.
51. Decanini LD, Liberatore L, Mollaioli F. Strength and stiffness reduction factors for infilled frames with openings. *Earthq Eng Eng Vib*. 2014;13:437-454.
52. Asteris PG, Cavaleri L, Di Trapani F, Sarhosis V. A macro-modelling approach for the analysis of infilled frame structures considering the effects of openings and vertical loads. *Struct Infrastruct Eng*. 2016;12(5):551-566.
53. ASCE/SEI 41. *Seismic Evaluation and Retrofit of Existing Buildings*. ASCE, 2013.
54. New Zealand Society for Earthquake Engineering (NZSEE). *Assessment and Improvement of the Structural Performance of Buildings in Earthquakes*. NZSEE; 2006.
55. GB 50011-2010. Chinese Code for Seismic Design of Buildings, Ministry of Housing and Urban-Rural Construction of People's Republic of China, Beijing, China, 2010.
56. Standard Test Methods for Sampling and Testing Brick and Structural Clay Tile, ASTM C67/C67M-19. ASTM International, 2018.
57. Standard Test Method for Compressive Strength for Laboratory Constructed Masonry Prisms, ASTM E 447- 97. American Society for Testing and Materials, 1997.
58. Cardone D, Perrone G. Developing fragility curves and loss functions for masonry infill walls. *Earthq Struct*. 2015;9(1):257-279.
59. Chiozzi A, Miranda E. Fragility functions for masonry infill walls with in-plane loading. *Earthq Engng Struct Dyn*. 2017;46(15):2831-2850.
60. Di Trapani F, Bolis V, Basone F, Preti MG. Seismic reliability and loss assessment of RC frame structures with traditional and innovative masonry infills. *Eng Struct*. 2020;208:110306.

How to cite this article: Di Trapani F, Khan NA, Zhou L, Demartino C, Monti G. Cyclic response of infilled RC frames with window and door openings: Experimental results and damage interpretation. *Earthquake Engng Struct Dyn*. 2023;1-25. <https://doi.org/10.1002/eqe.4005>